ResearchGate

See discussions, stats, and author profiles for this publication at: https://www.researchgate.net/publication/230830036

Scale morphology and flexibility in the shortfin mako Isurus oxyrinchus and the blacktip shark Carcharhinus limbatus

Article *in* Journal of Morphology · October 2012

DOI: 10.1002/jmor.20083 · Source: PubMed

CITATIONS
27

READS
561

5 authors, including:

Philip Motta
University of South Florida
151 PUBLICATIONS **3,758** CITATIONS
SEE PROFILE

Maria Laura Habegger
University of South Florida
11 PUBLICATIONS **186** CITATIONS
SEE PROFILE

Amy Lang
University of Alabama
60 PUBLICATIONS **163** CITATIONS
SEE PROFILE

Jessica Davis
University of South Florida
1 PUBLICATION **27** CITATIONS
SEE PROFILE

Some of the authors of this publication are also working on these related projects:

Actuation of 2D microflaps in the lower region of the boundary layer View project

Feeding mechanics of fishes View project

All content following this page was uploaded by Maria Laura Habegger on 28 September 2017.

The user has requested enhancement of the downloaded file.

Scale Morphology and Flexibility in the Shortfin Mako *Isurus oxyrinchus* and the Blacktip Shark *Carcharhinus limbatus*

Philip Motta,[1]* Maria Laura Habegger,[1] Amy Lang,[2] Robert Hueter[3] and Jessica Davis[1]

[1]*Department of Integrative Biology, University of South Florida, Tampa, Florida 33620*
[2]*Department of Aerospace Engineering, University of Alabama, Tuscaloosa, Alabama 35487*
[3]*National Center for Shark Research, Mote Marine Laboratory, Sarasota, Florida 34236*

ABSTRACT We quantified placoid scale morphology and flexibility in the shortfin mako *Isurus oxyrinchus* and the blacktip shark *Carcharhinus limbatus*. The shortfin mako shark has shorter scales than the blacktip shark. The majority of the shortfin mako shark scales have three longitudinal riblets with narrow spacing and shallow grooves. In comparison, the blacktip shark scales have five to seven longitudinal riblets with wider spacing and deeper grooves. Manual manipulation of the scales at 16 regions on the body and fins revealed a range of scale flexibility, from regions of nonerectable scales such as on the leading edge of the fins to highly erectable scales along the flank of the shortfin mako shark body. The flank scales of the shortfin mako shark can be erected to a greater angle than the flank scales of the blacktip shark. The shortfin mako shark has a region of highly flexible scales on the lateral flank that can be erected to at least 50°. The scales of the two species are anchored in the stratum laxum of the dermis. The attachment fibers of the scales in both species appear to be almost exclusively collagen, with elastin fibers visible in the stratum laxum of both species. The most erectable scales of the shortfin mako shark have long crowns and relatively short bases that are wider than long. The combination of a long crown length to short base length facilitates pivoting of the scales. Erection of flank scales and resulting drag reduction is hypothesized to be passively driven by localized flow patterns over the skin. J. Morphol. 000:000–000, 2012. © 2012 Wiley Periodicals, Inc.

KEY WORDS: dermal denticles; placoid scales; dermis; collagen; elastin; drag

INTRODUCTION

The earliest record of elasmobranch fishes is from isolated shark scales that date back to the late Ordovician period, about 455 million years ago (Janvier, 1996; Sansom et al., 1996; Ahlberg, 2001). These placoid scales (dermal denticles) accommodate bioluminescent and sensory organs, and are purported to serve a variety of functional roles including mechanical and biological protection, abrasion resistance, and parasite protection as well as antifouling, hydrodynamic drag reduction and increased thrust (Reif, 1985a,b; Bechert et al., 1986; Raschi and Musick, 1986; Raschi and Tabit, 1992; Carman et al., 2006; Schumacher et al., 2007a,b). Mounting evidence indicates that drag reduction most likely occurs by reducing turbulent crossflow near the scale surface, thereby reducing shear stress, and by control of flow separation around the body, which would reduce pressure drag (Bechert et al., 1997b, 2000; Lang et al., 2008, 2011, in press). In addition, increased thrust may occur on the fins by reducing the leading edge vortex thereby increasing anteriorly directed suction (Oeffner and Lauder, 2012).

Elasmobranch skin is composed of a thin epidermis sitting upon a thick dermis. The dermis is divided into a superficial stratum laxum (S. spongiosum/S. vasculare/S. superficiale) and a deeper stratum compactum. The stratum compactum of sharks, which is the better studied of the two layers, is composed of type I collagen fibers arranged in a lamellar fashion. Each layer comprises helically wound and parallel fibers, with alternate layers lying at the same angle (Fig. 1; Kimura et al., 1981; Lingham-Soliar, 2005a,b; Hwang et al., 2007; Meyer and Seegers, 2012). The helically wound fibers course around the body forming angles of ~50–70° to the longitudinal axis

Additional Supporting Information may be found in the online version of this article.

Contract grant sponsor: Collaborative National Science Foundation; Contract grant number: 0932352, 0744670, and 0931787; Contract grant sponsors: The University of South Florida and The Porter Family Foundation.

*Correspondence to: Philip Motta, Department of Integrative Biology, University of South Florida, 4202 East Fowler Ave., Tampa, Florida 33620.
E-mail: motta@usf.edu

Received 24 January 2012; Revised 25 April 2012;
Accepted 6 May 2012

Published online in
Wiley Online Library (wileyonlinelibrary.com)
DOI: 10.1002/jmor.20047

© 2012 WILEY PERIODICALS, INC.

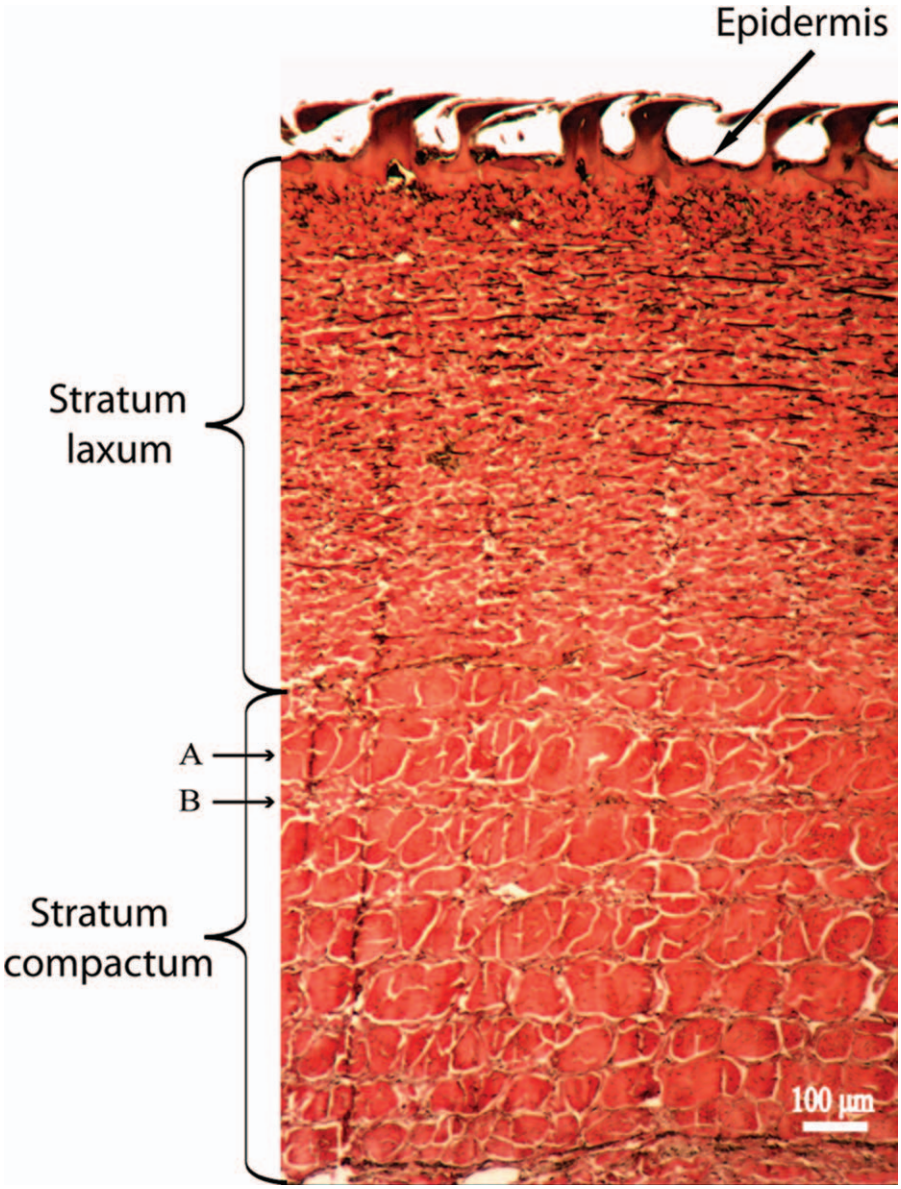

Fig. 1. Sagittal section through the skin of a 192 cm TL female shortfin mako shark *Isurus oxyrinchus* in the H2 region of the body showing the stratum laxum and stratum compactum regions of the dermis relative to the thin epidermis and marginal scales. Collagen fibers are stained red and elastin fibers black. Elastin fibers are primarily found in the stratum laxum. A, B, examples of two adjacent cross-helically wound fiber layers in the stratum compactum.

(Motta, 1977; Wainwright et al., 1978). In elasmobranchs, elastin fibers may be dispersed among the collagen fibers of the dermal layers (Naresh et al., 1985, 1997). Situated upon this pressurized exoskeleton of collagenous dermal fibers (Wainwright et al., 1978; Martinez et al., 2002), the placoid scales are found in a variety of shapes and sizes that vary both interspecifically and even across the body of perhaps all species of sharks (Sayles and Hershkowitz, 1937; Bigelow and Schroeder, 1948; Reif, 1985a; Raschi and Tabit, 1992; Bargar and Thorson, 1995; Deynat, 2005).

The gross anatomy of placoid scales varies immensely; however, they all consist of a crown, neck, and base (Fig. 2). An enameloid layer overlies dentin which extends from the crown down into the neck. A putative bony base, or bone of attachment, is embedded within the stratum laxum by attachment fibers (Sharpey's fibers) which supposedly course down into the deeper stratum compactum. A pulp cavity lies within the scales (Harder, 1975; Miyake et al., 1999; Lingham-Soliar, 2005a,b; Sire et al., 2009).

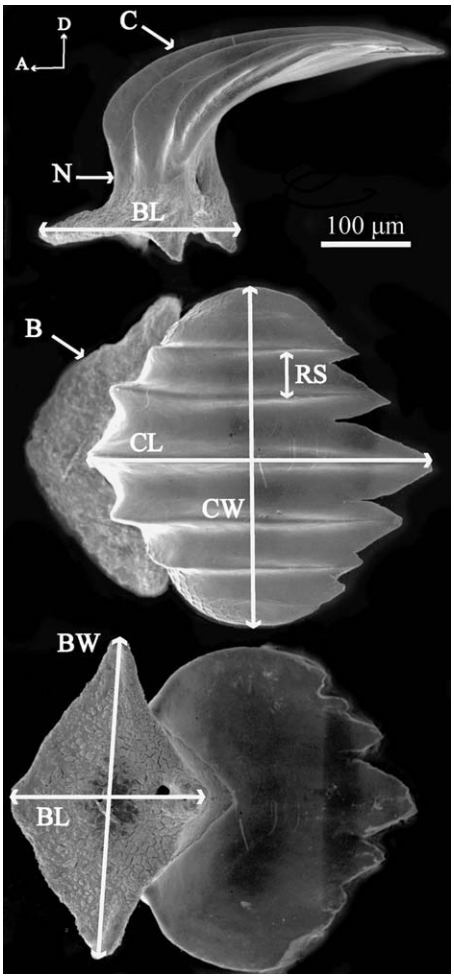

Fig. 2. Lateral, dorsal and ventral view of a placoid scale (dermal denticle) from a 135.5 cm TL female blacktip shark *Carcharhinus limbatus* from the B2 region of the body. Morphometric measures are indicated on each view (magnification 200X). Dorsal and anterior is indicated for the upper, lateral view. B, base; BL, base length; BW, base width; C, crown; CL, crown length; CW, crown width; N, neck; RS, riblet spacing.

The morphology of the scale crown varies considerably not only across the body but also among species. The majority of scales on faster swimming sharks such as the shortfin mako *Isurus oxyrinchus*, blacktip shark *Carcharhinus limbatus*, and silky shark *Carcharhinus falciformis* have a series of parallel riblets (also termed micro-ridges, ridges, or keels) that run in an anterior–posterior direction, often terminating in cusps on the trailing edge of the scale (Fig. 2). Because the orientation of these riblets is very specific, even around sensory organs, it has long been assumed they have a hydrodynamic role (Reif and Dinkelacker, 1982; Reif, 1985c; Bechert et al., 1986; Raschi and Musick, 1986; Bushnell and Moore, 1991). Within the fastest swimming sharks the height (~30 μm) and spacing (~40–80 μm) of the riblets is quite consistent, and sharks such as *I. oxyrinchus* and *C. falciformis* can alter the angle of attack of the scales relative to the skin, although the mechanism is unknown (Bechert et al., 1985; Lang et al., 2011, in press). In these sharks scale pliability may be related to basal plate size reduction and therefore less firm anchoring in the dermis (Porter and Evers, 1982; Reif, 1985a; Raschi and Musick, 1986; Raschi and Tabit, 1992; Lang et al., 2011, in press).

To date, however, there have been no studies that have both fully characterized the morphology of the scales on a fast and slower swimming shark, and simultaneously measured the possible angles of erection together across the body. The goals of this study were to: 1) Measure scale erection angles of the shortfin mako *I. oxyrinchus*, a fast-swimming shark species, and the slower swimming blacktip shark *C. limbatus*; 2) describe the morphology of the scales; 3) describe the histology of scale attachment to the skin; and 4) investigate the putative mechanism for increased scale flexibility at certain regions of the shortfin mako body by comparing scale morphology across the bodies of the shortfin mako and blacktip shark.

MATERIAL AND METHODS

Species, Collection, and General Measurements

The shortfin mako *Isurus oxyrinchus* is a coastal and oceanic open water predatory shark that attains a maximum total length (TL) of ~400 cm (Compagno et al., 2005). It is one of the fastest swimming sharks (Carey and Teal, 1969; Reif, 1985a; Stevens, 2009). It is also one of the species to have flexible scales over large portions of its body (Bechert et al., 1985; Bruse et al., 1993; Lang et al., 2011, in press). The blacktip shark *Carcharhinus limbatus* is a coastal shark that grows to a maximum TL of ~255 cm (Compagno et al., 2005), attaining a lower maximum burst velocity than the shortfin mako, at least during jumping (Brunnschweiler, 2005).

Three shortfin mako sharks *I. oxyrinchus* (female TL 192 cm, fork length [FL] 171.5 cm; male TL 158 cm, FL 150 cm; male TL 171.5 cm, FL 166 cm), and three blacktip sharks *C. limbatus* (male TL 142 cm, FL 119 cm; female TL 135.5 cm, FL 107.5 cm; female TL 155 cm, FL 137cm) were collected in 2010 by commercial and recreational fishers. The first two shortfin mako sharks were used in our preliminary study (Lang et al., 2011). Shortfin mako sharks were collected in the Atlantic coastal waters off Montauk, New York, and blacktip sharks in the Gulf of Mexico off Florida. The specimens were wrapped tightly in plastic bags to minimize desiccation and frozen until measurements were taken. Tissue harvesting was approved under the University of South Florida Institutional Animal Care and Use Committee (IACUC) protocol numbers T 3839 and T 3253, as well as Mote Marine Laboratory IACUC number 09-09-PM2.

Following Reif (1985a), placoid scales at sixteen regions along the body were marked to sample scales under a variety of flow regimes (Fig. 3). Three 1 cm^2 samples from each location were removed, two for histological analysis and one for scanning electron microscopy (SEM).

Angle Measurements

Because swimming sharks have superambient subcutaneous pressure ranging from 20-200 kPa (Wainwright et al., 1978; Martinez et al., 2002), scale erection angles were recorded with

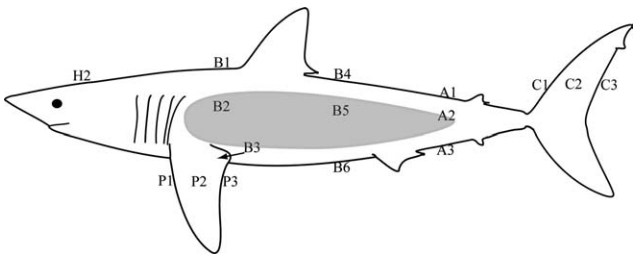

Fig. 3. Lateral view of a shortfin mako *Isurus oxyrinchus* showing the regions sampled. The general region with the greatest scale flexibility ($\geq 50^{\circ}$) is shaded in gray on the flank of the shark. Modified from Lang et al. (2011).

and without superambient subcutaneous pressure on the first two shortfin mako and blacktip sharks. The methods outlined here follow that of Lang et al. (2011) with the addition of the third shortfin mako shark and the blacktip sharks. Initially we wanted to determine if superambient subcutaneous pressure resulted in scale erection. Two shortfin mako sharks (female 192 cm TL, male 158 cm TL) and two blacktip sharks (male 142 cm TL, female 135.5 cm TL) were placed under a Meiji EMZ-TR stereo microscope at 135X magnification. In seven of the sixteen regions (B1, B2, B4, B5, A1, A2, A3), a hard plastic sheet (to distribute the load) was placed over a folded infant aneroid sphygmomanometer inflated to 103 kPa. An ocular calibrated reticle in the microscope was used to measure the erection angle, if any, of one to three individually marked scales before and after inflation (Lang et al., 2011). Scale erection (without manual manipulation) due to pressure change did not occur in either of the two shortfin mako or two blacktip sharks in any region tested, so testing proceeded to the next step.

Under superambient subcutaneous pressure of 103 kPa, five haphazardly selected scales in each of the regions B1, B2, B4, B5, A1, A2, A3 were gently manipulated with a fine acupuncture needle to the maximum resting erection angle (the angle they would remain at after removal of the needle) on the former two shortfin mako and two blacktip sharks, and their erection angles were measured. In all cases, the manually erected scales were left to settle in place with no movement before they were measured, and they were not manually erected to the extent that their base was torn from the skin. The pressure was then released and the angle similarly calculated on five different scales on the flaccid skin. For the majority of regions, there was no difference in mean erection angles between the two methods (see Results). Therefore, to expedite the process and be consistent, on the third shortfin mako (male 171.5 cm TL) and third blacktip shark (female 155 cm TL), the skin was inflated to mimic stretching the skin as before but the angles were measured only after the pressure was released from the sphygmomanometer. At the other regions (H2, B3, B6, P1, P2, P3, C1, C2, C3) where subcutaneous pressure was not possible, the erection angles were measured on all six sharks by gently erecting the scales (if possible) with the acupuncture needle. Being concerned that cutting and then stretching the skin could affect the dermis and hence erectability of the scales, the erection angles of 10 scales in two regions (B2 and B4) on the male TL 171.5 cm shortfin mako were measured by manipulation before the skin was cut or stretched, and then after the skin had been cut, inflated and the pressure released. There was no difference in angles of either region (see Results).

Finally, 35 equidistant sampling locations encompassing the entire dorsal, left lateral, and ventral surfaces of each shark from the region adjacent to the third gill slit to the second dorsal fin origin were marked and one to three scales in each area manually erected as before without subcutaneous pressure, and the erected angle subjectively assessed as being either approximately greater or less than 50° by two researchers independently. If the angle was close to 50° but ambiguous, the angle was quantified as above.

From histological and fresh tissue samples of the skin and scales, scanning electron micrographs of the scales, and isolated scales, the crown length and width, base length and width (measured to 5–8 μm accuracy), as well as riblet spacing (1-μm accuracy) and depth (2-μm accuracy) were measured. Measurements were taken by ocular micrometer with an Olympus IM compound microscope at 100–400X and a Meiji EMZ-TR stereo microscope at 135X magnification on two to three sharks of each species. Measurements from digital copies of the SEM photographs were made with Sigma Scan Pro 4 software (SYSTAT Software).

Tissue Processing SEM

Unstretched skin samples with placoid scales were first rinsed in an ultrasonic cleaner with water for ~30 s. Tissue samples were then fixed with 2.5% glutaraldehyde in 0.1 mol l^{-1} phosphate buffer (pH 7.2 at 4°C) for 7 days. After fixation, samples were rinsed with water several times to remove buffer salts. Dehydration of the tissue was performed by the application of a consecutive series of increased concentrations of ethanol (35, 70, 95, and 100%) for ~15 min each. After dehydration, the tissue was immersed for 10 min in 100% hexamethyldisilazane, and the procedure repeated two times. Finally, samples were air-dried under a vacuum. Samples were sputter-coated and examined under a JEOL JSM-35 scanning electron microscope at 10 kV, and pictures taken with Fuji FP-100B45 film at magnifications from 100 to 300X, as well as a Topcon Aquila scanning electron microscope at 10 kV, with digital pictures taken at 100 and 200x. Isolated scales from all regions of the body were prepared by soaking pieces of skin in ~2.5% sodium hypochlorite solution in an ultrasonic cleaner for ~3–4 min, after which the individual scales were transferred to SEM plugs.

Tissue Processing Histology

Additional unstretched skin samples were removed from the frozen shark and stored in 10% buffered formalin. After fixation, samples were decalcified in a formic acid (50% HCOOH, 50 % H_20) -sodium citrate (500 g $NaH_2C_6H_5O_7$, 2500 ml H_20) solution for seven to ten days. Sections of 4 μm were prepared in a Bioacut microtome (Leica/Reichert Jung, model 2030) and stained using the Verhoeff-Van Gieson (VVG) Staining Protocol (Sigma-Aldrich©, Accustain elastic stain Procedure No. HT25). Slides were examined and photographed under an Olympus IM compound microscope from 40 to 200X with a MD 900 AmScope digital camera.

Statistics

The mean erection angles of 10 scales in the B2 and B4 regions of the 171.5 cm TL shortfin mako shark were compared before and after stretching the skin with a Mann-Whitney rank sum test. Mean erection angles with and without the application of pressure were compared statistically for each of the seven regions for the first two individuals of each species with a Tukey's HSD test. The angles of erection from all 16 regions (without subcutaneous pressure) of the body were compared intra-specifically on three individuals of each species. A randomized complete block design in the GLM procedure was used to test the effect of shark (block) against area on the body (treatment) for first the shortfin mako and then the blacktip sharks. This test determined that the three sharks of each species did not differ intra-specifically so the three sharks for each species were combined. Post hoc multiple comparisons t tests in the GLM procedure determined a region of greater scale flexibility along the flank of the shortfin mako shark (B2, B5, A2), therefore further regional comparisons were performed for areas of the body combined. Regional analyses were performed in three main areas of the body (dorsal B1, B4, A1; lateral B2, B5, A2; and ventral regions B3, B6, A3). These tests were per-

TABLE 1. Morphometric measurements from scales of three shortfin mako sharks Isurus oxyrinchus *(Female 192 cm TL, Male 171.5 cm TL, Male 158 cm TL) and two blacktip sharks* Carcharhinus limbatus *(Male 142 cm TL, Female 135.5 cm TL)*

Region	H2	B1	B2	B3	B4	B5	B6	A1	A2	A3	P1	P2	P3	C1	C2	C3
Isurus oxyrinchus																
CL (μm)	217 ± 6	218 ± 1	221 ± 7	220 ± 8	208 ± 4	202 ± 4	208 ± 3	199 ± 3	221 ± 6	299 ± 1	295 ± 2	205 ± 1	191 ± 5	232 ± 1	193 ± 5	169 ± 4
CW(μm)	183 ± 5	189 ± 5	167 ± 3	155 ± 5	180 ± 5	149 ± 3	152 ± 3	149 ± 3	175 ± 10	213 ± 5	244 ± 8	159 ± 4	139 ± 4	199 ± 9	146 ± 7	140 ± 4
BL (μm)	181 ± 8	166 ± 11	78 ± 6	126 ± 7	160 ± 7	74 ± 4	109 ± 5	145 ± 4	100 ± 7	259 ± 8	264 ± 14	154 ± 9	128 ± 10	217 ± 12	172 ± 9	139 ± 3
BW (μm)	196 ± 5	194 ± 10	158 ± 5	156 ± 7	182 ± 8	147 ± 6	147 ± 9	154 ± 2	172 ± 9	221 ± 13	218 ± 13	156 ± 5	141 ± 4	183 ± 12	139 ± 13	129 ± 7
RD (μm)	2 ± 0	7 ± 0	8 ± 0	12 ± 0	10 ± 0	7 ± 0	12 ± 0	11 ± 0	10 ± 0	0 ± 0	0 ± 0	8 ± 2[a]	6 ± 0	0 ± 0	7 ± 0	7 ± 0
RS (μm)	39 ± 1	39 ± 1	43 ± 1	39 ± 1	39 ± 1	43 ± 1	37 ± 1	36 ± 1	45 ± 1	N/A	N/A	34 ± 1	35 ± 1	N/A	33 ± 1	29 ± 1
RD/RS[b]	0.1	0.2	0.2	0.3	0.2	0.2	0.3	0.3	0.2	N/A	N/A	0.2	0.2	N/A	0.2	0.2
CL/CW	1.2 ± 0.0	1.2 ± 0.0	1.3 ± 0.0	1.4 ± 0.0	1.2 ± 0.0	1.4 ± 0.0	1.4 ± 0.0	1.3 ± 0.0	1.3 ± 0.1	1.4 ± 0.1	1.2 ± 0.1	1.3 ± 0.1	1.4 ± 0.0	1.2 ± 0.1	1.3 ± 0.1	1.2 ± 0.1
BL/BW	0.9 ± 0.0	0.9 ± 0.1	0.5 ± 0.1	0.8 ± 0.0	0.9 ± 0.1	0.5 ± 0.0	0.8 ± 0.1	0.9 ± 0.0	0.6 ± 0.0	1.2 ± 0.1	1.2 ± 0.1	1.0 ± 0.1	0.9 ± 0.1	1.2 ± 0.1	1.3 ± 0.1	1.1 ± 0.1
CL/BL	1.2 ± 0.1	1.3 ± 0.1	2.9 ± 0.3	1.8 ± 0.1	1.3 ± 0.1	2.8 ± 0.2	1.9 ± 0.1	1.4 ± 0.1	2.2 ± 0.1	1.2 ± 0.0	1.1 ± 0.0	1.3 ± 0.1	1.5 ± 0.1	1.1 ± 0.0	1.1 ± 0.1	1.2 ± 0.0
Carcharhinus limbatus																
CL (μm)	369 ± 7	378 ± 5	362 ± 13	340 ± 13	414 ± 10	394 ± 10	375 ± 19	426 ± 4	412 ± 14	380 ± 12	435 ± 9	384 ± 10	273 ± 6	398 ± 26	371 ± 12	166 ± 5
CW(μm)	393 ± 13	420 ± 16	396 ± 12	340 ± 7	493 ± 5	461 ± 13	380 ± 14	483 ± 10	483 ± 22	318 ± 19	329 ± 4	336 ± 7	191 ± 7	366 ± 24	363 ± 19	172 ± 10
BL (μm)	317 ± 10	301 ± 10	222 ± 6	229 ± 13	357 ± 7	264 ± 16	267 ± 10	374 ± 15	297 ± 7	276 ± 12	384 ± 9	326 ± 14	166 ± 10	380 ± 16	336 ± 23	111 ± 7
BW (μm)	429 ± 13	444 ± 13	416 ± 12	358 ± 8	548 ± 5	474 ± 27	396 ± 9	532 ± 5	492 ± 16	378 ± 16	264 ± 5	364 ± 7	183 ± 6	357 ± 18	380 ± 9	148 ± 8
RD (μm) (lateral)	5 ± 1	10 ± 1	10 ± 1	10 ± 1	15 ± 1	19 ± 1	15 ± 1	15 ± 1	15 ± 1	16 ± 1	0 ± 0	6 ± 0	4 ± 0	0 ± 0	6 ± 0	0 ± 0
RD (μm) (medial)	6 ± 1	14 ± 1	13 ± 1	14 ± 1	19 ± 1	25 ± 1	20 ± 1	17 ± 1	18 ± 1	21 ± 1	0 ± 0	9 ± 1	6 ± 1	0 ± 0	7 ± 1	0 ± 0
RS (μm) (lateral)	54 ± 2	50 ± 1	55 ± 1	48 ± 1	67 ± 2	64 ± 1	51 ± 1	59 ± 1	63 ± 1	54 ± 1	N/A	38 ± 1	37 ± 1	N/A	46 ± 1	N/A
RS (μm) (medial)	61 ± 2	63 ± 1	73 ± 1	58 ± 1	80 ± 2	82 ± 1	60 ± 1	70 ± 2	83 ± 1	65 ± 1	N/A	48 ± 1	34 ± 1	N/A	51 ± 2	N/A
RD/RS (lateral)[b]	0.1	0.2	0.2	0.2	0.2	0.3	0.3	0.3	0.2	0.3	N/A	0.2	0.1	N/A	0.1	N/A
RD/RS (medial)[b]	0.1	0.2	0.2	0.2	0.2	0.3	0.3	0.2	0.2	0.3	N/A	0.2	0.2	N/A	0.1	N/A
CL/CW	0.9 ± 0.0	0.9 ± 0.0	0.9 ± 0.0	1.0 ± 0.0	0.8 ± 0.0	0.9 ± 0.0	1.0 ± 0.0	0.9 ± 0.0	0.9 ± 0.0	1.2 ± 0.0	1.3 ± 0.0	1.1 ± 0.0	1.4 ± 0.0	1.1 ± 0.1	1.0 ± 0.1	1.0 ± 0.1
BL/BW	0.7 ± 0.0	0.7 ± 0.0	0.5 ± 0.0	0.6 ± 0.0	0.7 ± 0.0	0.6 ± 0.0	0.7 ± 0.0	0.7 ± 0.0	0.6 ± 0.0	0.7 ± 0.0	1.5 ± 0.1	0.9 ± 0.0	0.9 ± 0.1	1.1 ± 0.1	0.9 ± 0.1	0.8 ± 0.1
CL/BL	1.2 ± 0.0	1.3 ± 0.0	1.6 ± 0.0	1.5 ± 0.1	1.2 ± 0.0	1.5 ± 0.1	1.4 ± 0.0	1.2 ± 0.0	1.4 ± 0.0	1.4 ± 0.0	1.1 ± 0.0	1.2 ± 0.0	1.7 ± 0.1	1.0 ± 0.0	1.1 ± 0.1	1.5 ± 0.1

Sampling regions are indicated in Figure 3. Riblet depth and spacing for the blacktip shark is taken from the most medial and adjacent lateral grooves as these scales have five riblets. With three riblets, the depth and spacing of the shortfin mako shark is taken from the groove adjacent to the central riblet. Ratios of the various measures are indicated. Values are means ± SE where indicated. BL, base length; BW, base width; CL, crown length; CW, crown width; RD, riblet depth; RS, riblet spacing.

[a]measured on individual removed scales.

[b]The ratio of ridge depth to ridge spacing is the ratio of two means and therefore has no SE. This is due to the two measures not being always taken from the same scale.

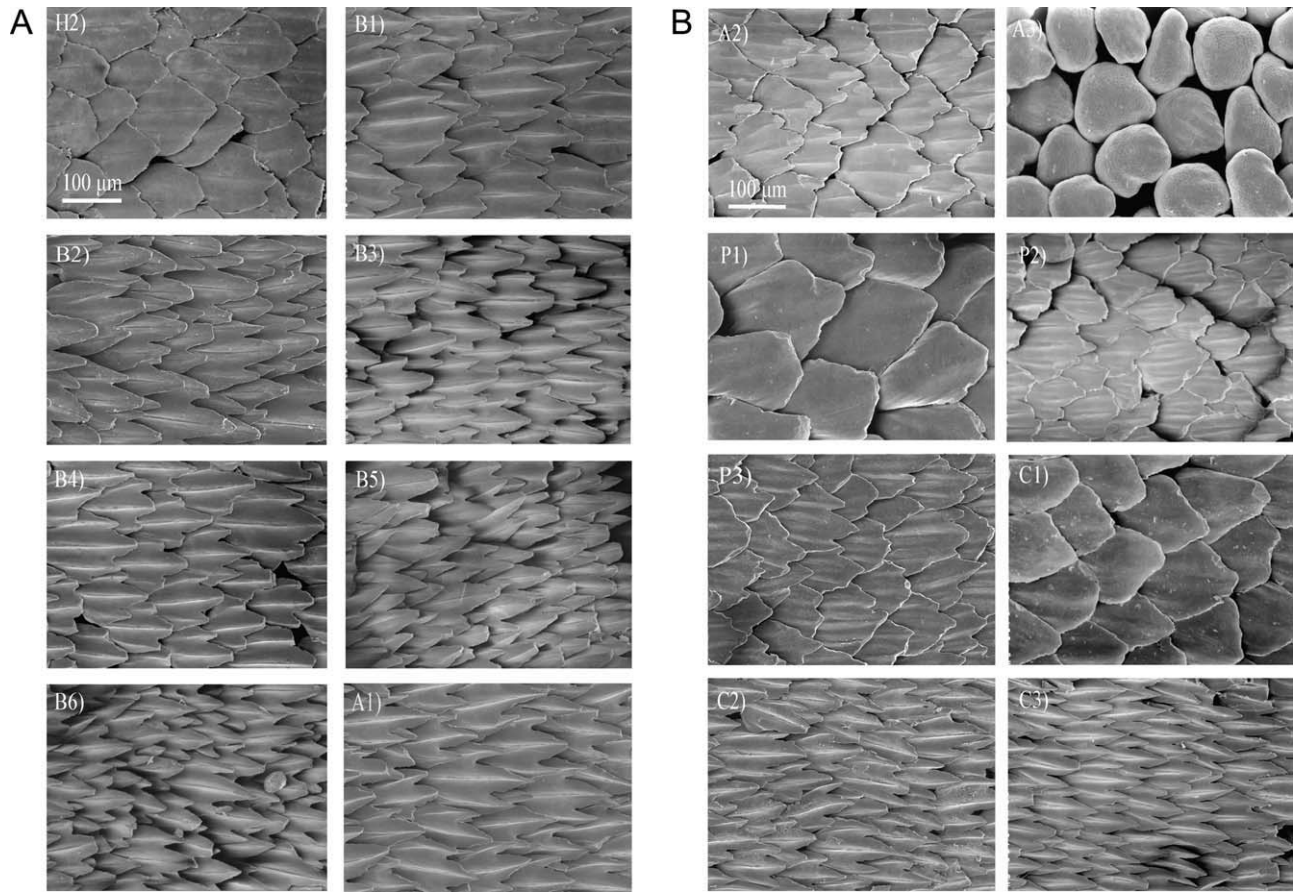

Fig. 4. Dorsal view of placoid scales from a 158 cm TL male shortfin mako *Isurus oxyrinchus* at the sixteen regions outlined in Figure 3 (magnification 200X). The scale crowns on regions P1, C1, and A3 are almost or completely smooth and lacking riblets; the crowns in regions B3, B6, A3 and B5 are long and narrow. Anterior is to the left.

formed with a Kruskal-Wallis one way ANOVA on ranks followed by a Tukey's pairwise multiple comparisons. Additional comparisons were performed between the dorsal, flank and ventral regions of the shortfin mako sharks to the same regions of the blacktip sharks, and finally the three regions of the pectoral fin (P1, P2, P3) were compared between species, as were the caudal fin regions (C1, C2, C3). These tests were performed with a Tukey's HSD test.

Normality and equality of variance, when applicable, were tested with the Shapiro-Wilk and Levene Median tests respectively. Statistical analyses were performed in SAS (version 9.2, SAS Institute, Cary, NC) or SigmaPlot (version 11.0, SYSTAT Software, Chicago, IL). Morphometric measures of the individual scales (length, width, and aspect ratios) were not statistically analyzed as the majority of measures were taken from only one or two sharks of each species. Statistical analysis was also not performed for the erection angles deemed to be greater than or equal to 50° for one to three scales in the 35 equidistant sampling locations.

RESULTS

Scale Morphology and Erection

***Isurus oxyrinchus*.** The majority of the placoid scales throughout the body had three longitudinal riblets with spacing ranging from 29 ± 1 to 45 ± 1 μm across the 16 measured regions of the body. The depth of the grooves between the riblets on the body ranged from 2 ± 0 μm on the dorsal head region H2 to 12 ± 0 μm in the ventral B3 and B6 regions. The ratio of riblet depth to spacing, which is equivalent to riblet height/spacing, was low and ranged from 0.1 to 0.3. Crown length ranged from 169 ± 4 to 299 ± 1 μm, and crown width from 139 ± 4 to 244 ± 8 μm (Table 1). The scales on the leading edge of the pectoral (P1), caudal fin (C1) and in front of the anal fin (A3) were almost smooth with only traces of riblets (Fig. 4).

The ratio of crown length to width was generally greatest for the ventral scales (B3, B6, A3) but was also large for the flank region B5 (indicating longer more narrow scales). However, the ratio of crown length to base length was greatest for the flank scales (B2, B5, A2) indicating that the flank scales had long crowns and relatively short bases. These flank scales also had the lowest base length to width ratios (~0.5) indicating that the flank scales had bases with large widths but short

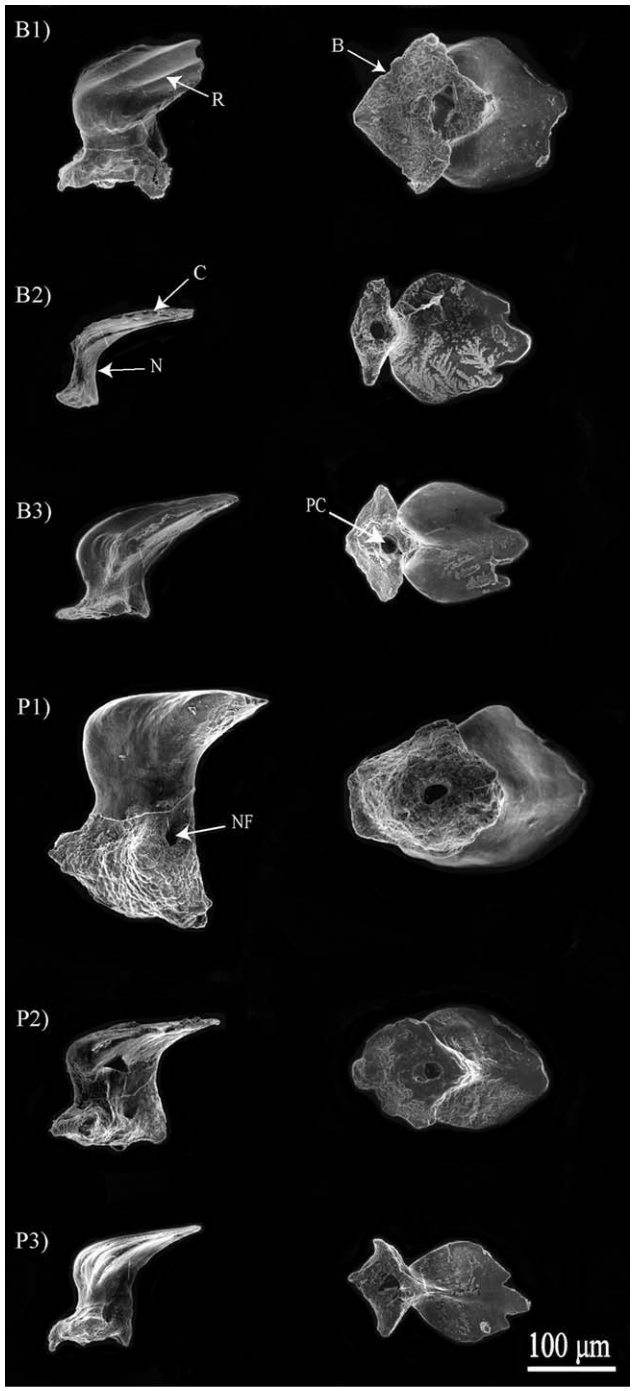

Fig. 5. Lateral and ventral views of representative placoid scales from a 158 cm TL male shortfin mako *Isurus oxyrinchus* at various regions: B1; B2; B3; P1; P2; P3. Note the relative length of the crown and base at the various regions, as well as the shape of the base, particularly at the B2 flank region which has long crowns and short bases, and a more triangular base compared to the more rhomboid bases of the other regions (magnification 300X). Anterior is to the left. B, base; C, crown; N, neck; NF, nutrient foramina; PC, pulp cavity; R, riblet.

lengths, being essentially triangular in shape. The bases of the other scales were more rhomboid in shape (Table 1; Fig. 5).

TABLE 2. Mean erection angles plus standard errors for the sixteen regions of the shortfin mako Isurus oxyrinchus *and the blacktip shark* Carcharhinus limbatus

	I. oxyrinchus **(*n*=3)**	***C. limbatus*** **(*n*=3)**
H2	33° ± 1	33° ± 2
B1	28° ± 1	30° ± 1
B2	48° ± 1	32° ± 1
B3	30° ± 1	33° ± 1
B4	25° ± 1	29° ± 2
B5	43° ± 2	32° ± 2
B6	28° ± 1	31° ± 1
A1	25° ± 1	29° ± 2
A2	39° ± 1	32° ± 2
A3	16° ± 3	29° ± 1
P1	1° ± 1	0° ± 0
P2	23° ± 1	23° ± 1
P3	32° ± 2	25° ± 1
C1	25° ± 2	0° ± 0
C2	28° ± 1	26° ± 1
C3	30° ± 2	40° ± 2

Stretching the skin in the B2 and B4 regions did not affect erection angles (T = 87.0, P = 0.185; T = 94.5, P = 0.447). Application of subcutaneous pressure up to 103 kPa did not result in scale erection. Out of seven regions, erection angles with and without pressure only changed for the B1 and B5 regions, being greater without pressure in both cases (Tukey HSD $P \leq 0.05$).

Comparison among the 16 regions on *I. oxyrinchus* without pressure determined no significant difference in erection angles among the three individual sharks, so they were combined (RCBD df = 2, F = 1.43, P = 0.256). The mean erection angles from the 16 body regions ranged from 1° ± 1 on the leading edge of the pectoral fin P1 to 48° ± 1 in the flank region B2 (Table 2). Post hoc tests determined a pattern of higher flexibility on the scales along the lateral (flank) region of the body (B2 = 48° ± 1, B5 = 43° ± 2, and A2 = 39° ± 1) (LSD df = 15, F = 33.76, $P < 0.0001$; Table 2). Consequently a regional analysis combining dorsum, flank and ventral regions of the body as well as pectoral and caudal fins was performed. The lateral scales (B2, B5, A2) had significantly greater erection angles (mean angle = 44° ± 1) than both the dorsal (mean angle = 26° ± 1) and ventral regions (mean angle = 25° ± 1). Erection angles for the dorsal region did not differ from that of the ventral region (Kruskal Wallis df = 2, H = 81.805, $P = \leq 0.001$; Tukey $P < 0.05$). The scales on the leading edge of the pectoral fin (P1; 1° ± 1) had significantly smaller erection angles than that of the central region of the fin (P2; 23° ± 1) as well as the trailing edge (P3; 32° ± 2). The latter two regions did not differ (Kruskal Wallis df = 2, H =35.058, $P = < 0.001$; Tukey $P < 0.05$). Conversely, for the caudal fin the mean angles were not significantly different among the three regions (C1, C2, C3; Kruskal Wallis df = 2, H = 5.524,

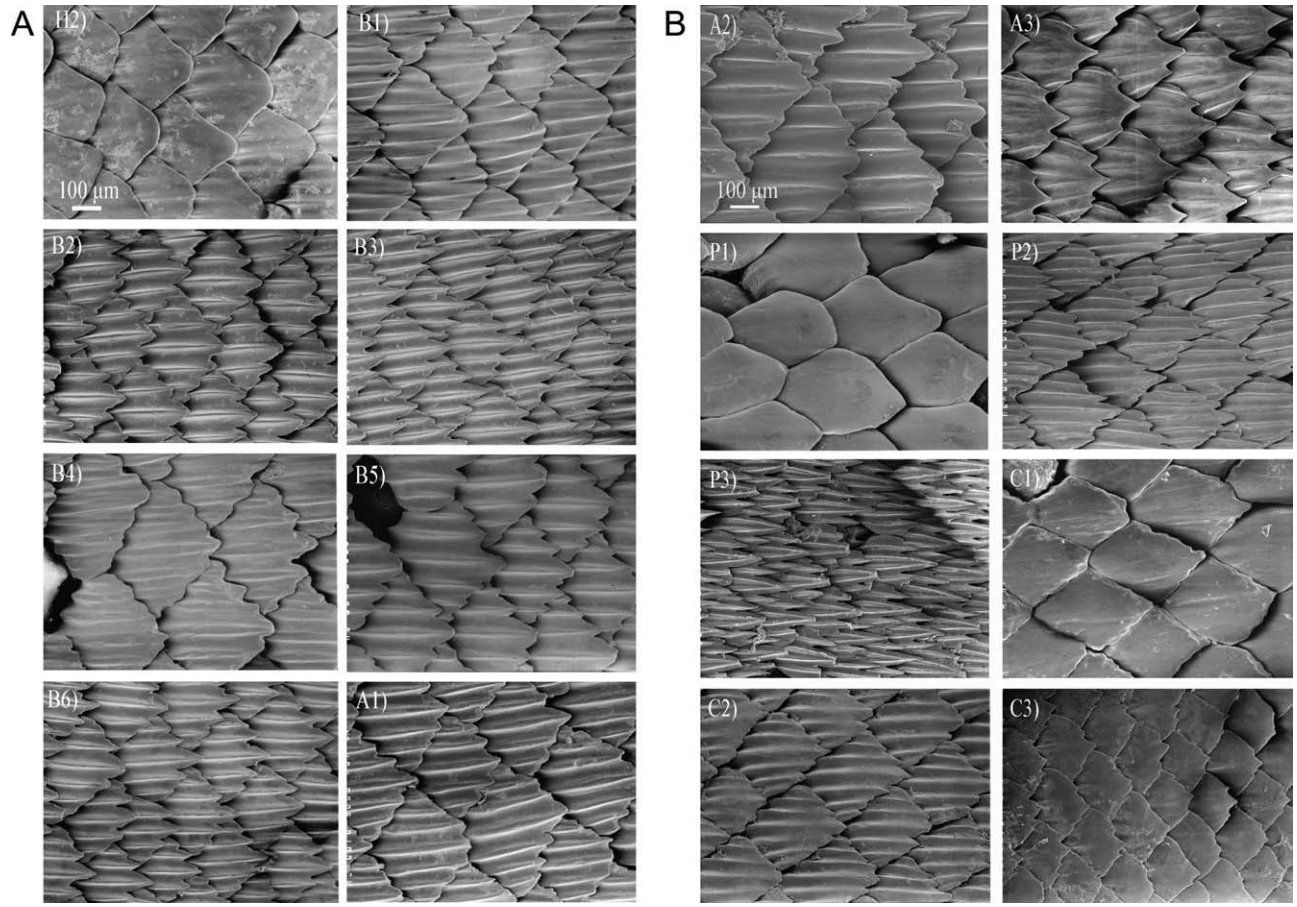

Fig. 6. Dorsal view of placoid scales from a 135.5 cm TL female blacktip shark *Carcharhinus limbatus* at the sixteen regions outlined in Figure 3 (magnification 100X). The scale crowns on P1 and C1 are essentially smooth and devoid of riblets, and C3 is almost smooth. The crowns on P3 are long and narrow. Anterior is to the left.

$P = 0.063$; Table 2). Mapping the erection angles across the entire body revealed a flank region of highly flexible scales that could be erected at least 50° (Fig. 3).

Carcharhinus limbatus. The placoid scales of the blacktip shark were much larger than those of the shortfin mako. The majority of the scales had 5–7 longitudinal riblets with an average spacing of 34 ± 1 to 83 ± 1 μm across the 16 regions of the body, and an average groove depth of 4 ± 0 to 25 ± 1 μm. The relative riblet heights were similar to those of the shortfin mako shark, with the riblet depth to spacing ratio ranging from 0.1 to 0.3 (Table 1). Pectoral and caudal fin leading edge scales were smooth, and trailing edge caudal fin scales only had traces of riblets (Fig. 6). Crown length throughout the body ranged from 166 ± 5 to 435 ± 9 μm, and crown width from 172 ± 10 to 493 ± 5 μm.

The ratio of crown length to width was greatest for scales on the trailing edge of the pectoral fin (P3), being very long and narrow. The ratio of crown length to base length was greatest for the trailing edges of the fins (P3, C3) as well as partly along the flank (B2 and B5) and the ventral regions (B3). The base length to base width aspect ratio was relatively consistent throughout the shark indicative of almost rhomboid-shaped bases, with the exception of the leading edge of the pectoral and caudal fin (P1, C1) which had large aspect ratios indicating scales with large, symmetrical and well anchored bases (Fig. 7, Table 1).

Application of subcutaneous pressure up to 103 kPa in seven regions of the body did not result in scale erection. Out of seven regions, erection angles with and without pressure only changed for the B4 and A1 regions, being greater without pressure in both cases (Tukey HSD $P \leq 0.05$).

Comparison among the 16 regions without pressure determined no significant difference in erection angles among the three individuals so they were combined (GLM df = 2, $F = 0.87$, $P = 0.429$). Post hoc tests determined some differences among regions with the majority of differences being confined to the leading edge of the pectoral fin P1 (0° ± 0) and caudal fin C1 (0° ± 0; LSD df = 15, F =

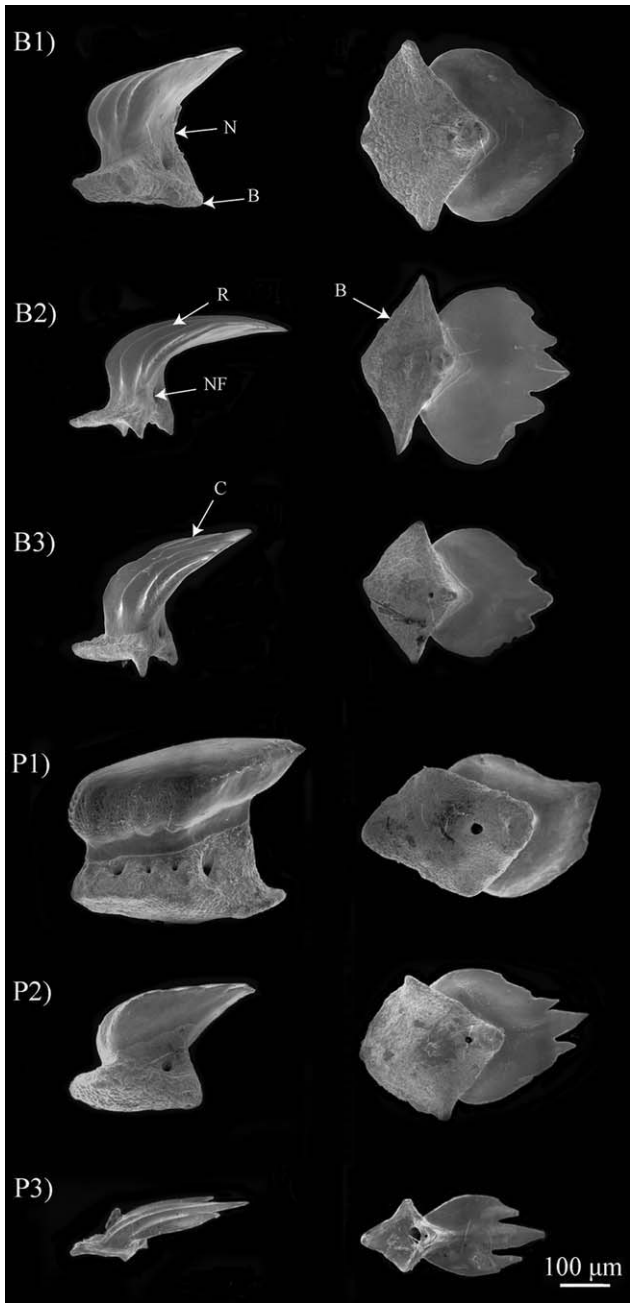

Fig. 7. Lateral and ventral views of representative placoid scales from a 135.5 cm TL female blacktip shark *Carcharhinus limbatus* at various regions: B1; B2; B3; P1; P2; P3. Note the relative length of the crown and base at the various regions (magnification 150X). The ratio of crown length to base length is large for P3, B2, B3, B5 and C3 (last two not shown). The bases of the scales are rhomboid in shape, and those of regions P1 and C1 (not shown) are especially large and well anchored. Anterior is to the left. B, base; C, crown; N, neck; NF, nutrient foramina; R, riblet.

17.91, $P < 0.0001$; Table 2). The mean erection angles from the 16 non-pressurized body regions ranged from 0° ± 0 (P1 and C1) to 40° ± 2 (C3; Table 2). To be consistent a regional analysis was also performed for this species. Statistical analysis showed no significant differences among the dorsal (mean angle = 30° ± 1; B1, B4, A1), flank (mean angle = 32° ± 1; B2, B5, A2) and ventral region of the body (mean angle = 31° ± 1; B3, B6, A3; Kruskal Wallis df = 2, $H = 3.29$, $P = 0.193$). The scales on the trailing edge of the pectoral fin (P3) had the highest erection angles (25° ± 1) compared to the leading edge (P1) (0° ± 0) and the central region of the fin (P2; 23° ± 1), however, only the leading edge (P1) was significantly different from the other two regions (Kruskal Wallis df = 2, $H = 30.925$, $P = <0.001$). On the caudal fin, however, all the regions were significantly different from each other, C1 (0° ± 0), C2 (26° ± 1) and C3 (40° ± 2; Kruskal Wallis df = 2, $H = 37.761$, $P < 0.001$). Mapping of scale erection angles equal to or greater than 50° indicated there were no regions with highly erectable scales as seen in the shortfin mako.

Interspecific comparison. Comparing erection angles between the shortfin mako and blacktip shark, those of the flank scales of the shortfin mako (B2, B5, A2) were significantly greater (mean angle = 44° ± 1) than the flank scales of the blacktip shark (mean angle = 32° ± 1). There was no difference between dorsal scale angles of the shortfin mako and blacktip shark, or between the ventral scale angles of the two species (Kruskal Wallis df = 5, $H = 115.199$, $P < 0.001$). Comparing similar regions in the fins between species, there was no difference in the three regions of the pectoral fin (Table 2; Kruskal Wallis df = 5, $H = 69.913$, $P < 0.001$). On the leading edge of the caudal fin (C1) the shortfin mako sharks had more erectable scales (25° ± 2) than the blacktip shark (0° ± 0). The mid and trailing edge scale angles of the caudal fin did not differ between species (Kruskal Wallis df = 5, $H = 56.632$, $P < 0.001$; Table 2).

Scale Histology

The placoid scales of the shortfin mako and blacktip sharks were anchored in the stratum laxum of the dermis with no obvious direct connection to the fibers of the stratum compactum. The attachment fibers of the scales in both species were almost exclusively collagen (Figs. 1, 8, and 9 red fibers). Elastin fibers (black) were visible in the stratum laxum of both species but were almost completely lacking in the dense, cross-helically wound fibers of the deeper stratum compactum (e.g., Fig. 1). The majority of elastin fibers were generally aligned with the longitudinal axis of the scales in the body region (e.g. Figs. 8, 9, B1 and B3). In both species, there were apparently less elastin fibers in the dermis of the pectoral (P1, P2, P3) and caudal fins (C1, C2, C3) as compared to

the body regions (B1, B2, B3), although not quantified (Figs. 8 and 9).

The lower crown length to base length ratio for the caudal fin scales of the shortfin mako shark are visible in Figure 8, regions C1 and C2, as well as in the blacktip shark (Fig. 9 C1 and C2). The epidermis was only a few cell layers thick in both species, with melanophores visible within it. Ceratotrichia were visible below the trailing edge scales of the pectoral fin (Figs. 8 C3 and 9 P3). The pavement-like scales on the leading edge of the pectoral fin of the blacktip shark were characterized by thick, closely spaced bases (Fig. 9 P1). The trailing edge scales of the blacktip shark pectoral fin had long thin crowns as compared to their bases. These scales were embedded in the stratum laxum overlying the cartilaginous ceratotrichia (Fig. 9 P3).

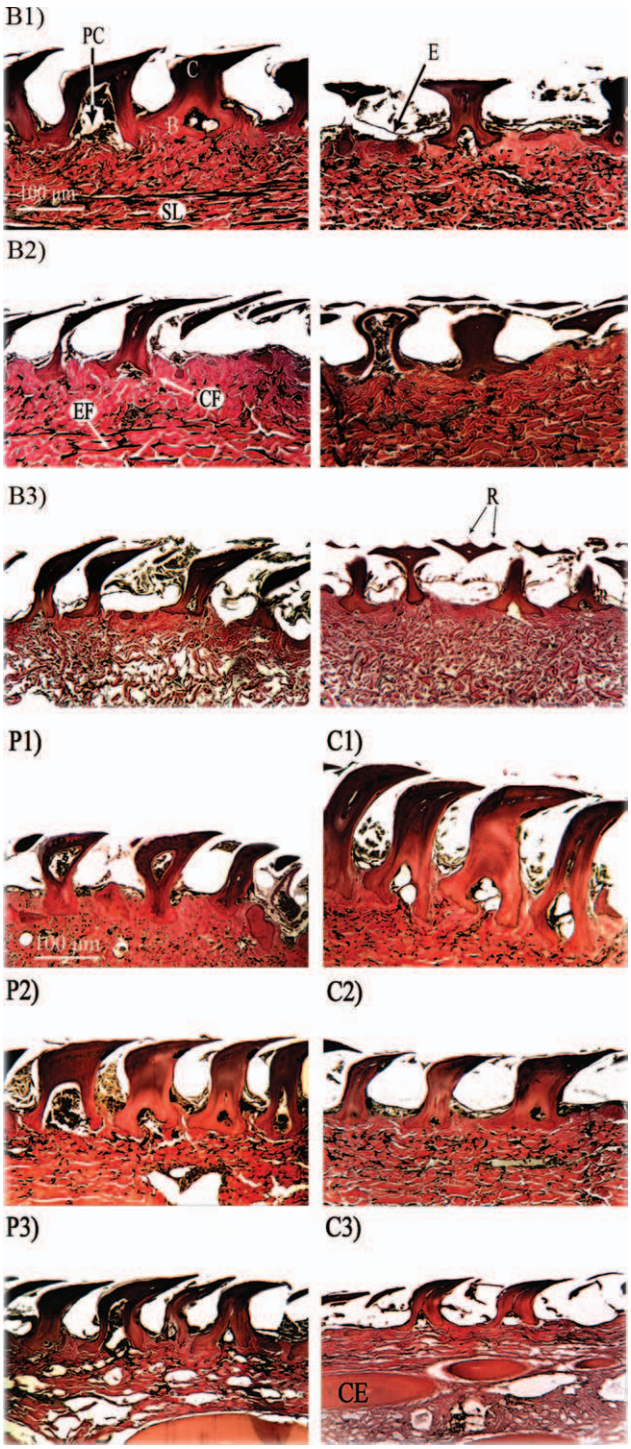

DISCUSSION

Erection Angles and Scale Shape

The shortfin mako *Isurus oxyrinchus*, one of the fastest swimming sharks, has a region of highly flexible scales along the flank with erection angles equal to or greater than 50° (Fig. 3, Table 2). This is in contrast to the scales on the other regions of the shortfin mako's body as well as all the scales of the blacktip shark *Carcharhinus limbatus*, which are not as erectable. These erection angles are most likely minimal estimates as the scales could be erected easily past these angles, but were only measured after they had returned to a "resting" position. These results support our preliminary findings on two shortfin mako sharks (Lang et al., 2011). Bechert et al. (1985) also noted greater scale flexibility in some fast-swimming sharks including the shortfin mako. We hypothesize that this region of erectable scales on the shortfin mako shark is related to its rapid burst swimming speed.

Shortfin mako sharks feed on teleost fishes as well as crustaceans and cephalopods in the North Atlantic. Predation upon larger and faster swim-

Fig. 8. Histological pictures of the skin (partial view) and the placoid scales from a 192 cm TL female shortfin mako *Isurus oxyrinchus* from the body regions B1, B2, B3 (B1 and B3 sagittal, B2 frontal, and B1, B2, B3 transverse sections); pectoral fin P1, P2, P3 (sagittal sections); and caudal fin C1, C2, C3 (frontal sections). Not all portions of each scale are visible due to the sectioning, and total crown or base length may not be accurate as the scales may not be cut exactly at their midpoint. The stratum compactum is not visible. The material between some of the scale crowns is epidermis and perhaps mucus (e.g. B3); slight separation of the epidermis is most likely due to histological preparation. The scale crowns in the flank region B2 are long compared to their bases, and together with wide but short triangular bases, give them greater flexibility on the skin. By comparison, the relatively short crowns and large bases of C1 result in firmly anchored scales. Numerous elastic fibers are visible in the stratum laxum of the body regions B1, B2, B3, and relatively less so in the pectoral and caudal fin (P1-P3, C1-C3), and the attachment fibers of the scales are almost exclusively collagen. Collagen is stained red and elastin black. B, base; C, crown; CE, ceratotrichia; CF, collagen fibers; E, epidermis; EF, elastin fibers; PC, pulp cavity; R, riblet; SL, stratum laxum of the dermis. Pictures B1 and B3 lateral modified from Lang et al. (2011).

ming fishes including swordfish (*Xiphias gladius*), striped marlin (*Tetrapturus audax*) and other sharks is not uncommon (Stillwell and Kohler, 1982; Maia et al., 2006; Castro, 2011). These sharks may also be preyed upon by white sharks *Carcharodon carcharias* (Fergusson et al., 2000), so rapid pursuit and escape are important factors in the evolution of this fast-swimming shark. Furthermore, the shortfin mako is an endothermic shark that retains metabolic heat for increased muscle power in certain regions of the body (Carey and Teal, 1969; Carey et al., 1981; Bernal et al., 2001; Sepulveda et al., 2004). Based on the height to which these fishes can jump out of the water, escape velocities of 9.8 m/s have been estimated (Carey and Teal, 1969). These sharks use thunniform swimming where the degree of lateral motion is confined to the more posterior end of the body. These sharks, like tuna, have the least lateral movement in their mid-body region (Donley et al., 2004), the region of greatest scale flexibility (Fig. 3, Table 2). Assuming a conservative maximum burst speed of only 10 body lengths/seconds (Blake, 1983), a 400-cm TL shortfin mako, which is the approximate maximum TL (Compagno et al., 2005), would attain speeds of ~4000 cm/s or 144 km/h, and a 200-cm TL shark would attain 72 km/h. These speeds translate into Reynold's numbers (Re) of 1.6×10^8 and 4×10^7, respectively. At these Reynold's numbers, the boundary layer is thinner and turbulent (Vogel, 2003). Consequently, Reif (1985a) considered the shortfin mako to be a fast pelagic hunting shark (his category a).

The blacktip shark *C. limbatus*, which is a coastal epibenthic predator, most likely has slower burst speeds. Other somewhat closely related carcharhinid sharks to *C. limbatus* ((whitetip reef shark *Triaenodon obesus*, blacktip reef shark *C. melanopterus*, grey reef shark *C. amblyrhynchos* [Vélez-Zuazo and Agnarsson, 2011]) are categorized by Reif (1985a) as large near-shore hunters (his category b) based on scale morphology, habitat use, and swim speed. Based on height of jumps out of the water, escape velocities of 6.4 m/sec have been calculated for *C. limbatus* (Brunnschweiler, 2005), supporting the notion that they do not attain as high swim speeds as *I. oxyrinchus*.

There are a variety of mechanisms whereby shark scales may reduce drag. The first involves

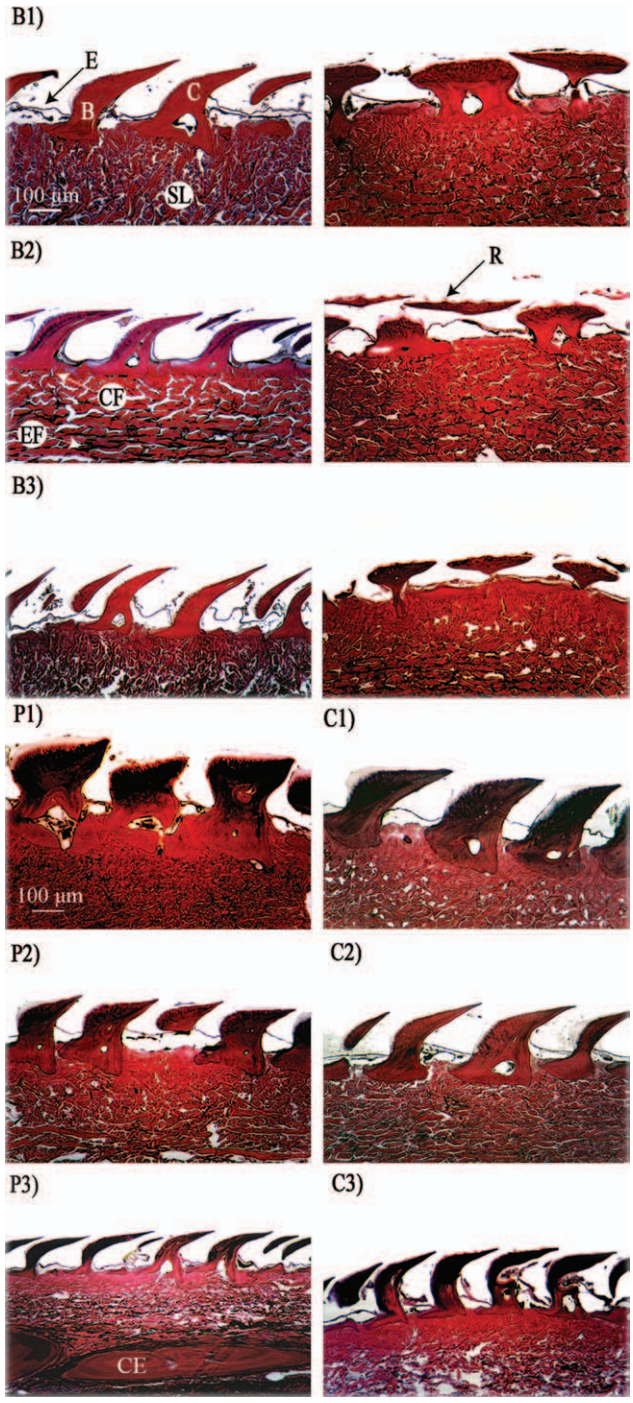

Fig. 9. Histological pictures of the skin (partial view) and the placoid scales from a 142 cm TL male blacktip shark *Carcharhinus limbatus* from the body regions B1, B2, B3 (B1, B3 sagittal, B2 frontal, and B1, B2, B3 transverse sections); pectoral fin P1, P2, P3 (sagittal sections); and caudal fin C1, C2, C3 (frontal sections). Not all portions of each scale are visible due to the sectioning, and total crown or base length may not be accurate as the scales may not be cut exactly at their midpoint. The stratum compactum is not visible. The material between some of the scale crowns is epidermis and perhaps mucus (e.g. C3); slight separation of the epidermis is most likely due to histological preparation. Numerous elastic fibers are visible in the stratum laxum of the body regions B1, B2, B3, and relatively less so in the pectoral and caudal fin (P1-P3, C1-C3) and the attachment fibers of the scales are almost exclusively collagen. The relatively large bases compared to the crowns of regions such as P1 and C1 result in firmly anchored scales that cannot be erected. Collagen is stained red and elastin black. B, base; C, crown; CE, ceratotrichia; CF, collagen fibers; E, epidermis; EF, elastin fibers; R, riblet; SL, stratum laxum of the dermis.

flow through the riblets that lie on the crown of the scales. On fast-swimming sharks, the scales have riblets that course in an approximate anterior-to-posterior direction. The spacing and height of these riblets is quite consistent, especially in the fastest swimming sharks (Reif, 1985a). Of 15 species of shark examined, Raschi and Musick (1986) report the shortfin mako to have the smallest scales. In our study, shortfin mako scales were almost consistently smaller than those of the blacktip shark, with generally longer and narrower crowns (CL/CW, Table 1, Figs. 4 and 6). Shortfin mako scales ranged from 169 to 299 μm in crown length, with longitudinal riblet spacing ranging between 29 and 45 μm and riblet height (depth) ranging from 2 to 12 μm. The spacing of the riblets was generally less than that of the blacktip shark which ranged from 34 to 83 μm (Table 1). Reif's (1985a) findings differ slightly, with an average riblet spacing distance of 40–45 μm for the shortfin mako, with a slight (12%) decrease in inter-ridge distance with ontogeny (however, sharks of only two sizes, 110 and 220 cm TL, were examined).

Longitudinal riblets reduce drag because they impede the fluctuating turbulent crossflow near the wall, and in this way reduce momentum transfer and shear stress. Under experimental conditions, an optimum riblet height/depth spacing of 0.7 reduced the shear stress with tests on scalloped riblets similar in shape to those on sharks (Bechert et al., 1997b; 2000). Neither the blacktip shark nor shortfin mako shark approach this optimal value, and even along the flank region of the shortfin mako shark (B2, B5, A2), the region with the most erectable scales, the ratio of riblet height/spacing is 0.2 (Table 1). Regardless, riblets do appear to reduce drag (Bechert et al., 2000). Interestingly, the slower swimming skates and rays lack riblets on their placoid scales (Deynat, 1999).

Another mechanism of reducing drag entails erection of the scales, either by active or passive means. Application of superambient subcutaneous pressure, under our experimental conditions, did not result in scale erection in either species. However, this must be taken with caution because this is not equivalent to superambient subcutaneous pressure resulting from muscle contraction (Wainwright et al., 1978; Martinez et al., 2002; Brainerd and Azizi, 2005; Flammang, 2010), nor does it consider the effects of muscle contraction on the adjacent myosepta, nor bending of the body.

We hypothesize that passive scale erection occurs along the flank of the shortfin mako. The erect scales may reduce drag by two methods. A passive, flow-actuated mechanism, due to the flexibility of the flank scales, can lead to control of flow separation around the shark's body. With increasing flow separation, pressure drag increases (Vogel, 2003). If the scales in the region of flow separation can erect, by either increases in subcutaneous pressure or passively due to flow reversal, they might stem the reversal of flow that occurs along the surface of the skin, thereby reducing pressure drag by controlling the process that leads to flow separation (Lang et al., 2011, in press).

Furthermore, a biomimetic model of shortfin mako shark scales erected to 90° confirmed the presence of embedded vortices between the scales, enhancing the mixing in the boundary layer (Lang et al., 2008; 2011). This would also help to keep the flow attached, and maintaining an attached flow reduces the overall drag (Bechert et al., 1985; Bechert et al., 2000). Controlling flow separation can therefore lead to a reduction in form or pressure drag during burst swimming and turning maneuvers. But what passive mechanism results in scale erection? Flow reversal occurs adjacent to the wall within a separating boundary layer. This reversed flow can exceed one third of the free stream velocity (Smith, 2011; Lang, personal observation). This temporary flow reversal may initiate scale erection. In a test at a lower Reynold's number (100,000), Smith (2011) found that fresh shortfin mako flank skin, with scales mounted to a NACA 4412 hydrofoil at 16° angle of attack under a turbulent boundary layer condition, significantly reduced the average thickness and magnitude of the region of separation. This provides strong evidence that even at this low Reynold's number the scales bristled and created a partial-slip condition.

The role that mucus plays in all of these mechanisms is unknown. Based on studies of *Scyliorhinus canicula*, sharks have well-developed mucus glands in their skin but little is known of their mucus production. In general, however, sharks appear to produce little mucus that may remain under the scales, and the faster swimming sharks such as the shortfin mako are believed to produce less mucus (Reif, 1980; Bechert et al., 1985; Reif, 1985a; Meyer and Seegers, 2012).

The scales on the leading edge of the fins of fast-swimming sharks are often smooth, which is believed to reduce skin friction on these surfaces that have a thinner boundary layer (Reif, 1985a). The scales on the leading edge of the pectoral (P1) and caudal fins (C1) of the shortfin mako are almost smooth with only traces of riblets, as are those on the blacktip shark. In contrast to the leading edge scales, some of the trailing edge scales are long, have elongated cusps, and are somewhat flexible in the shortfin mako and blacktip shark (Figs. 4 and 6). These trailing edge scales may also act as self-activated movable flaps to increase lift and retard flow separation over the fins. The optimal design for such flaps includes a jagged or scalloped edge such as seen on the trailing edge scales of the shortfin mako caudal fin

(Fig. 4) and blacktip shark pectoral fin (Fig. 6) (Bechert et al., 1997a; Schatz et al., 2004).

Scale Attachment and Flexibility

Critical to the hypothesis that the scales are erected passively is scale flexibility along the flank of the shortfin mako, the region most prone to flow separation. Increased scale flexibility in this shark appears to be related to two things, the increased crown to base length, and the shape of the base. The ratio of crown length to base length was greatest for the flank scales (B2, B5, A2) of the shortfin mako shark, indicating that the flank scales have long crowns and relatively short bases (Table 1; Fig. 8 B2). These flank scales also had the lowest base length-to-width ratios ($\sim$0.5) being triangular in shape. In contrast, the bases of the other scales are more rhomboid in shape (Fig. 5). In the blacktip shark the scale base length to base width aspect ratio was relatively consistent throughout the shark, again indicative of almost rhomboid shaped bases (Table 1, Fig. 7). The flexible flank scales of the shortfin mako shark therefore have greater leverage with their long crowns and short bases should a reverse flow occur on the skin (Supporting Information Figs. S-1 and S-2). Furthermore, the more triangular base of these flank scales pivot about their axis running through the relatively short but wide base, whereas the more rhomboid and broad-based scales on other regions of the body more firmly anchor these scales.

The placoid scales of *I. oxyrinchus* and *C. limbatus* are exclusively anchored to the collagen fibers of the stratum laxum with no obvious attachment to fibers of the stratum compactum (Figs. 1, 8, and 9). In all of the histological slides there are no obvious (from their black staining) elastic fibers attached to the base of the scales, and the elastic fibers appear to be almost exclusively found in the more superficial stratum laxum in both species. This is in contrast to the findings of Naresh et al. (1985) who stated that elastin fibers were not found in the stratum laxum of rays but were instead sparsely distributed in the stratum compactum. Although not quantified, there appears to be more elastin fibers in the body regions of the shortfin mako and blacktip sharks than in the dermis of the pectoral and caudal fins (Figs. 8 and 9). Therefore, return of the shortfin mako shark placoid scales from their erected position is most likely due to straightening out of the bundles of collagen fibers and stretching of the individual crimped collagen fibrils (so-called toe region of the collagen stress-strain curve) (Diamant et al., 1972; Roeder et al., 2002) and perhaps deformation of the superficial stratum laxum with its elastic fibers oriented in the direction of the scale crowns.

In summary, the shortfin mako *I. oxyrinchus* has a flank region of highly erectable and loosely attached scales as compared to the scales on other parts of its body and to those of the blacktip shark *C. limbatus*. These scales can be manually erected to angles of at least 50°, whereas scales on other regions of the body such as the leading edges of some of the fins are nonerectable. The scales of the shortfin mako shark are generally shorter and narrower than those of the blacktip shark, and the riblet pattern of the shortfin mako shark scales differs from that of the blacktip shark by being more closely spaced and shallower in depth. The bases of the very erectable flank scales of the shortfin mako are more triangular in shape and easily pivoted about their wide but short base, whereas those on most of the remainder of the shortfin mako's body and those of the blacktip shark tend to be more rhomboid in shape and broader based. The scales of both species are anchored into the more superficial stratum laxum of the dermis by collagen fibers. We hypothesize that the erectable nature of the placoid scales along the flanks of the shortfin mako shark allows a reduction of flow reversal, backflow, and pressure drag as this fast-swimming shark maneuvers through the water column.

ACKNOWLEDGMENTS

We are very thankful to Paul and Jane Majeski and crew, Captain Mark Sampson, Captain Al VanWormer, Captain Kevin Deiter, Philip Pegley, Blake Augsburger, Jack Morris, and Mote Marine Laboratory for providing shark specimens. Candy Miranda provided the exceptional histological work; Ed Haller demonstrated patience and a depth of knowledge on the SEM. Bruce Cowell, Jason Rohr and Christian Wells provided generous statistical advice. Sincere thanks to the three reviewers that who made this a better manuscript.

LITERATURE CITED

Ahlberg PEE. 2001. Major Events in Early Vertebrate Evolution: Palaeontology, Phylogeny, Genetics and Development. New York: Taylor & Francis. 418 p.

Bargar TW, Thorson TB. 1995. A scanning electron microscopy study of the dermal denticles of the bull shark, *Carcharhinus leucas*. J Aquaricul Aquat Sci 7:120–137.

Bechert DW, Bartenwerfer M, Hope G. 1986. Drag reduction mechanisms derived from shark skin. AIAA 15th Congress of the International Council of the Aeronautical Sciences. London, England. pp 1044–1068.

Bechert DW, Bruse M, Hage W, Meyer R. 1997a. Biological surfaces and their technological application- laboratory and flight experiments on drag reduction and separation control. 28th AIAA Fluid Dynamics Conference, Snowmass Village, CO. pp 1–34.

Bechert DW, Bruse M, Hage W, Meyer R. 2000. Fluid mechanics of biological surfaces and their technological application. Naturwissenschaften 87:157–171.

Bechert DW, Hoppe G, Reif WE. 1985. On the drag reduction of the shark skin. AIAA Shear Flow Control Conference. Boulder, CO. pp 1–18.

Bechert DW, Bruse M, Hage W, Van der Hoeven JGT, Hoppe G. 1997b. Experiments on drag-reducing surfaces and their optimization with adjustable geometry. J Fluid Mech 338:59–87.

Bernal D, Dickson KA, Shadwick RE, Graham JB. 2001. Review: analysis of the evolutionary convergence for high performance swimming in lamnid sharks and tunas. Comp Biochem Physiol A Comp Physiol 129:695–726.

Bigelow HB, Schroeder WC. 1948. Lancelets, cyclostomes, sharks. In: Tee-Van J, Breder C, Hildebrand S, Parr A, Schroeder W, editors. Fishes of the Western North Atlantic, Part 1, Mem. Sears Found Mar. Res. New Haven: Yale University Press. pp 98–177.

Blake RW. 1983. Fish Locomotion. Cambridge: Cambridge University Press. 208 p.

Brainerd EL, Azizi E. 2005. Muscle fiber angle, segment bulging and architectural gear ratio in segmented musculature. J Exp Biol 208:3249–3261.

Brunnschweiler JM. 2005. Water-escape velocities in jumping blacktip sharks. J R Soc Interface 2:389–391.

Bruse M, Bechert DW, Van Der Hoeven JGT, Hage W, Hoppe G. 1993. Experiments with conventional and novel adjustable drag-reducing surfaces. Proceedings of the International Conference. Tempe, AZ. pp 719–738.

Bushnell DM, Moore KJ. 1991. Drag reduction in nature. Annu Rev Fluid Mech 23:65–79.

Carey FG, Teal JM. 1969. Mako and porbeagle: warm bodied sharks. Comp Biochem Physiol 28:199–204.

Carey FG, Teal JM, Kanwisher JW. 1981. The viscera temperatures of mackerel sharks (Lamnidae). Physiol Zool 54:334–344.

Carman ML, Estes TG, Feinberg AW, Schumacher JF, Wilkerson W, Wilson LH, Callow ME, Callow JA, Brennan AB. 2006. Engineered antifouling microtopographies- correlating wettability with cell attachment. Biofouling 22:11–21.

Castro JI. 2011. The Sharks of North America. New York: Oxford University Press. 613 p.

Compagno LJV, Dando M, Fowler SL. 2005. Sharks of the World. New Jersey: Princeton University Press. 368 p.

Deynat PP. 1999. Dermal denticle morphology within batoid rays: a review. In: Se' ret BS, J.-Y., editors. Proceedings of the 3rd Meeting of the European Elasmobranch Association. Paris. pp 15–27.

Deynat PP. 2005. Characteristics of the dermal covering in Platyrhinidae (Chondrichthyes, Rhinobatiformes). Biociencias (Porto Alegre) 13:75–84.

Diamant J, Keller A, Baer E, Litt M, Arridge RGC. 1972. Collagen: ultrastructure and its relation to mechanical properties as a function of ageing. Proc R Soc Lond B Biol Sci 180:293–315.

Donley JM, Sepulveda CA, Konstantinids P, Gemballa S, Shadwick RE. 2004. Convergent evolution in mechanical design of lamnid sharks and tuna. Nature 429:61–65.

Fergusson IK, Compagno LJV, Marks MA. 2000. Predation by white sharks, *Carcharodon carcharias*, (Chondrichthyes: Lamnidae) upon chelonians, with new records from the Mediterranean Sea and a first record of the ocean sunfish *Mola mola* (Osteichthyes: Molidae) as stomach contents. Environ Biol Fishes 58:447–453.

Flammang BE. 2010. Functional morphology of the radialis muscle in shark tails. J Morphol 271:340–352.

Harder W. 1975. The Anatomy of Fishes. Stuttgart: E. Schweizerart'sche Verlagsbuchhandlung. 612 p.

Hwang JH, Mizuta S, Yokoyama Y, Yoshinaka R. 2007. Purification and characterization of molecular species of collagen in the skin of skate (*Raja kenojei*). Food Chem 100:921–925.

Janvier P. 1996. Early Vertebrates. Oxford: Oxford University Press. 393 p.

Kimura S, Kamimura T, Takema Y, Kubota M. 1981. Lower vertebrate collagen. Evidence for Type I-like collagen in the skin of lamprey and shark. Biochim Biophys Acta 669:251–257.

Lang A, Habegger ML, Motta P. Shark skin drag reduction. In: Bhushan B, editor. Encyclopedia of Nanotechnology, Dordrecht: Springer. (in press). DOI- 10.1007/978-90-481-9751-4_266.

Lang AW, Motta P, Hidalgo P, Westcott M. 2008. Bristled shark skin: A microgeometry for boundary layer control? Bioinsp Biomim 3:1–9.

Lang A, Motta P, Hueter R, Habegger M. 2011. Shark skin separation control mechanisms. J Mar Technol Soc 45:208–215.

Lingham-Soliar T. 2005a. Dorsal fin in the white shark, *Carcharodon carcharias*: a dynamic stabilizer for fast swimming. J Morphol 263:1–11.

Lingham-Soliar T. 2005b. Caudal fin in the white shark, *Carcharodon carcharias* (Lamnidae): a dynamic propeller for fast, efficient swimming. J Morphol 264:233–252.

Maia A, Queiroz N, Correia JP, Cabral H. 2006. Food habits of the shortfin mako, *Isurus oxyrinchus*, off the southwest coast of Portugal. Environ Biol Fish 77:157–167.

Martinez G, Drucker E, Summers A. 2002. Under pressure to swim fast. Integr Comp Biol 42:1273–1274.

Meyer W, Seegers U. 2012. Basics of skin structure and function in elasmobranchs: a review. J Fish Bio 80:1940–1967.

Miyake T, Vaglia JL, Taylor LH, Hall BK. 1999. Development of dermal denticles in skates (Chondrichthyes, Batoidea): Patterning and cellular differentiation. J Morphol 241:61–81.

Motta PJ. 1977. Anatomy and functional morphology of dermal collagen fibers in sharks. Copeia 1977:454–464.

Naresh MD, Das DK, Ramanathan N. 1985. A study on the histology of ray fish skin. Leath Sci 32:99–106.

Naresh MD, Arumugam V, Sanjeevi R. 1997. Mechanical behaviour of shark skin. J Biosci 22:431–437.

Oeffner J, Lauder GV. 2012. Hydrodynamic function of shark skin and two biomimetic applications. J Exp Biol 215:785–795.

Porter IM, Evers PM. 1982. The use of dermal denticle characteristics in shark identification. Electron Microscop Soc S Afr 12:83–84.

Raschi WG, Musick JA. 1986. Hydrodynamic aspects of shark scales. NASA CR 3963. pp 1–110.

Raschi W, Tabit C. 1992. Functional aspects of placoid scales: A review and update. Aust J Mar Fresh Res 43:123–147.

Reif WE. 1980. Development of dentition and dermal skeleton in embryonic *Scyliorhinus canicula*. J Morphol 166:275–288.

Reif WE. 1985a. Squamation and ecology of sharks. Cour Forsch-Inst Senckenberg 78:1–255.

Reif WE. 1985b. Functions of scales and photophores in mesopelagic luminescent sharks. Acta Zool Stockh 66:111–118.

Reif WE. 1985c. Morphology and hydrodynamic effect of the scales of fast swimming sharks. Fortschr Zool 30:483–485.

Reif WE, Dinkelacker A. 1982. Hydrodynamics of the squamation in fast swimming sharks. N Jb Geol Palaont Abh 164:184–187.

Roeder BA, Kokini K, Sturgis JE, Robinson JP, Voytik-Harbin SL. 2002. Tensile mechanical properties of three-dimensional I collagen extracellular matrices with varied microstructure. J Biomech Eng 124:214–222.

Sansom IJ, Smith MM, Smith PM. 1996. Scales of thelodont and shark-like fishes from the Ordovician of Colorado. Nature 379:628–630.

Sayles LP, Hershkowitz SG. 1937. Placoid scale types and their distribution in *Squalus acanthias*. Biol Bull 73:51–66.

Schatz M, Knacke T, Thiele F, Meyer R, Hage W, Bechert DW. 2004. Separation control by self-activated movable flaps. 42nd AIAA Aerospace Sciences Meeting and Exhibit, Reno, NV. pp 1–12.

Schumacher JF, Aldred N, Callow ME, Finlay JA, Callow JA, Clare AS, Brennan AB. 2007a. Species-specific engineered antifouling topographies: correlations between the settlement of algal zoospores and barnacle cyprids. Biofouling 23:307–317.

Schumacher JF, Carman ML, Estes TG, Feinberg AW, Wilson LH, Callow ME, Callow JA, Finlay JA, Brennan AB. 2007b. Engineered antifouling microtopographies- effect of feature size, geometry, and roughness on settlement of zoospores of the green alga *Ulva*. Biofouling 23:55–62.

Sepulveda CA, Kohin S, Chan C, Vetter R, Graham JB. 2004. Movement patterns, depth preferences, and stomach temperatures of free-swimming juvenile mako sharks, *Isurus oxyrinchus*, in the Southern California Bight. Mar Biol 145:191–199.

Sire J-Y, Donoghue PCJ, Vickaryous MK. 2009. Origin and evolution of the integumentary skeleton in non-tetrapod vertebrates. J Anat 214:409–440.

Smith JA. 2011. Turbulent separation control effects of mako shark skin samples on a NACA 4412 hydrofoil [thesis]. Tuscaloosa (AL): University of Alabama. 63 p.

Stevens J. 2009. The biology and ecology of the shortfin mako shark, *Isurus oxyrinchus*. In: Camhi MD, Pikitch EK, Babcock EA, editors. Sharks of the Open Ocean: Biology, Fisheries and Conservation. Oxford, UK: Blackwell Publishing Ltd. pp 87–94.

Stillwell CE, Kohler NE. 1982. Food, feeding habits, and estimates of daily ration of the shortfin mako (*Isurus oxyrinchus*) in the northwest Atlantic. Can J Fish Aquat Sci 39:407–414.

Vélez-Zuazo X, Agnarsson I. 2011. Shark tales: A molecular species-level phylogeny of sharks (Selachimorpha, Chondrichthyes). Molec Phylog Evol 58:207–217.

Vogel S. 2003. Comparative Biomechanics: Life's Physical World. Princeton: Princeton University Press. 580 p.

Wainwright SA, Vosburgh F, Hebrank JH. 1978. Shark skin: Function in locomotion. Science 202:747–749.

View publication stats